

# FORMATION OF A TYPICAL FORM OF AN OBJECT IMAGE IN A SERIES OF DIGITAL FRAMES

**Vadym Savanevych**

Doctor of Technical Sciences, Professor

Department of Systems Engineering\*\*

**Sergii Khlamov**

Corresponding author

PhD, Test Automation Lead

SoftServe

Sadova str., 2D, Lviv, Ukraine, 79021

E-mail: sergii.khlamov@gmail.com

**Vladimir Vlasenko**

PhD

Space Research and Communications Center\*\*\*

**Zhanna Deineko**

PhD, Associate Professor\*

**Oleksandr Briukhovetskyi**

PhD

Western Center of Radiotechnical Surveillance\*\*\*

**Iryna Tabakova**

PhD, Associate Professor\*

**Tetiana Trunova**

Engineer\*

\*Department of Media Systems and Technologies\*\*

\*\*Kharkiv National University of Radio Electronics

Nauky ave., 14, Kharkiv, Ukraine, 61166

\*\*\*National Space Facilities Control and Test Center

Moskovska str., 8, Kyiv, Ukraine, 01010

A computational method for the automated formation of a typical form of a digital image of the investigated objects on a series of digital frames has been developed. Due to the imperfection of the mounting of digital cameras, as well as their automated mounts, their immobility at shooting during exposure time can be disturbed, which leads to the formation of "blurred" images of objects of various forms.

Due to such inaccuracies in the tracking of objects on digital frames, even in one series, the typical form of the image of objects can vary from frame to frame. This fact of the difference in the standard form significantly complicates the execution of various image processing tasks.

In order to simplify the evaluation of the image parameters of objects in a series of digital frames, it has been proposed to use a typical image on a digital frame corresponding to the average image of objects as a model of object images. In this case, the appearance of the image of the object, its form, the distribution of brightness in the image will be determined only by the typical image.

This paper proposes a computational method for the automated formation and evaluation of the typical form of the image of an object in a digital frame based on the initial data – the actual given digital frame. This computational method is based on the selection of single images of objects and the formation of their rectangular area. Next, the offset is evaluated, and the selected single images of objects are normalized to calculate the typical form of the object image.

Using the method makes it possible to highlight objects against the background of noise and reduce the number of false detections. It is recommended to apply the method only in the case when the frames have defects and "blurs" during the shooting, otherwise there will be unreasonable additional computational costs.

The developed computational method was successfully tested in practice within the framework of the CoLiTec project and implemented in the intraframe processing unit of the Lemur software

**Keywords:** transfer function, OLS-evaluation of parameters, linear correlation coefficients, typical image form

Received date 06.10.2022

Accepted date 08.12.2022

Published date 30.12.2022

**How to Cite:** Savanevych, V., Khlamov, S., Vlasenko, V., Deineko, Z., Briukhovetskyi, O., Tabakova, I., Trunova, T. (2022). Formation of a typical form of an object image in a series of digital frames. *Eastern-European Journal of Enterprise Technologies*, 6 (2 (120)), 51–59.

doi: <https://doi.org/10.15587/1729-4061.2022.266988>

## 1. Introduction

Imperfections in the mounting of charge-coupled devices (CCDs) [1], digital cameras, and their automated mounting of telescopes leads to unintentional disturbances of immobility at shooting during exposure time. Features of the formation of various typical forms on CCD frames [2] is the violation of the telescope observational mode and the formation of "blurred" images of objects.

Due to such inaccuracies in the accompaniment of the objects under study on CCD frames of even one series, the typical form of their image can vary from frame to frame. This fact of the difference in the typical form of images of objects on a series of CCD frames significantly complicates the execution of various tasks of image processing and machine vision [3]. In addition, the accumulation of archival big

data [4] suggests that the acquisition of knowledge and subsequent analysis of historically accumulated data significantly improve the accuracy and quality of processing [5]. Therefore, it is a relevant task to develop a computational method for the automated formation of a typical form of a digital image of the objects under study on a series of CCD frames.

The theoretical value of this method includes a more accurate assessment of the image parameters [6] of both point and "blurred" objects. The practical value is to reduce the number of false detections, increasing the conditional probability of correct detection (CPCD) of real objects [7]. This fact will also simplify the identification of actual objects with already known celestial objects of the Solar System (SSO) [8] from the list of those cataloged in international astrometric databases [9], as well as in virtual observatories [10].

---

## 2. Literature review and problem statement

---

A variety of typical forms of images of objects can be the result of incorrect choice of the mode of telescope guiding (daily observation or tracking an object), disruption/failure of daily guidance, gusts of wind, or involuntary shift of a fixed CCD camera. This leads to synchronous elongation (the same directions and lengths of blurred images) of all images of the studied objects on the frame, which is a measure of significant blurring. Because of this significant blurring, the typical forms of images of the same objects under study may differ from frame to frame in the series. Blurring is significant only when the movement of the image of the object over the entire time of exposure cannot be neglected. In the case when the images of SSO (meteors, asteroids, comets) [11] are blurred due to their own motion, then this blur is not significant.

Thus, the blurring of the image of the studied objects, as well as the difference in their typical form from frame to frame in the series, significantly affect the accuracy of the image processing and machine vision tasks [12]. For example, the accuracy of astrometry [6], photometry [13], and motion detection [14] of the studied SSO using catalogs [15]. These high-level processing tasks make it possible to use only digital images with clear boundaries and a single brightness peak in the center as input data. However, they do not provide for the processing of blurred images.

This fact affects the segmentation of the image [16] due to the presence of different lengths of images on different frames. This leads to a different number of segments in the typical image of the object under study and requires additional analysis and filtering of segments. Therefore, the disadvantage of image segmentation methods is the inability to fully analyze only those segments and pixels that potentially belong to the typical image of the object under study [17].

Blurred CCD frames significantly affect the detection [18] and pixelation [19] of images of objects, as well as their recognition [20] and classification [21]. The disadvantage of such image processing methods is the fact that the boundaries of the typical image from frame to frame are fuzzy and different. This leads to the fact that the evaluation of the parameters of typical images of objects [3] in each frame becomes inaccurate and varies greatly from frame to frame in the series. This fact affects the total standard deviation (RMS) for the frame and the series as a whole. In addition, the difference in the typical form of the image of the object from frame to frame in the series significantly affects the detection of its movement and the assessment of the parameters of the trajectory of movement [6]. The disadvantage is the fact that the typical images of single objects are located in the intra-frame processing area (IFPA), which has different sizes from frame to frame.

Methods of addition of frames [22] can be used only when a typical image of the object under study is visible with clear boundaries on all CCD frames of the series. However, this is not possible when using the original data with a blurred image. Numerical methods based on Hawke, Radon transformations or their modifications [23, 24] are not able to detect a typical image of a blurred object with the required conditional probability of correct detection (CPCD). In addition, the accuracy of estimating image parameters by methods of analyzing signals and data [25], including the Wavelet transformation (analysis) [26], does not correspond to even the lowest threshold for accuracy in the absence of clear boundaries of the typical image of the object.

As the initial data, a digital frame is selected, on which, as a result of intra-frame processing,  $N_S$  single images of objects are detected. The image data contain random additive noise with a normal Gaussian distribution [27]. Images of single objects are within the IFPA. At the same time, the  $m$ -th IFPA is a set of  $\Omega_{Sm}$  of  $N_{Sm}$  pixels. Accordingly, the problem statement implies the formation and evaluation of the typical form of the image of the object on the digital frame on the basis of the initial data from the same digital frame.

---

## 3. The aim and objectives of the study

---

The purpose of this study is to form a typical form of a digital image of the objects under study on CCD frames. This will make it possible to use the average image of the object as an image model of all objects on each CCD frame in the series. It will also make it possible to standardize the typical form of the image of the object on all frames and more accurately evaluate its parameters.

To accomplish the aim, the following tasks have been set:

- to select single images of objects and exclude images distorted by coma from the list;
- to form a rectangular area of selected single images of objects with the subsequent assessment of their displacement, as well as normalize single images of objects based on the choice among them those with maximum intra-frame correlation;
- to develop a computational method for the automated formation of a typical form of the object image on a series of digital frames.

---

## 4. The study materials and methods

---

The object of our study is digital images of various objects on CCD frames, which can take a variety of typical forms. Within the framework of this study, the basic hypothesis put forward assumes that it is possible to obtain, on the basis of the initial data on the entire series of CCD frames, the corresponding average image of the object. This will allow it to be used as an image model (typical form) of objects on each CCD frame of the series. This typical form of the object image can be further used when performing basic image processing tasks by known methods. And the result of such processing will have a significant increase in the CPCD of images of objects, as well as the accuracy of estimating their parameters.

The obtained research results, as well as the developed computational method for the automated formation of a typical form of a digital image of objects on a series of CCD frames, were converted into a program code. The C++ programming language was used. This code was integrated into the system unit of intraframe processing of the Lemur software (Ukraine) [28] within the framework of the CoLiTec project [29].

The statistical method was chosen as the theoretical method of research. The efficiency criterion was used, which was calculated as the RMS difference between the experimental and model brightness of the pixels of the typical image of the blurred object on the frame. As an experimental study, full-scale experiments were conducted to determine the effectiveness of using a typical image of the object using

CCD frames of the telescopes KOS “Sazhen-S” (Dunaivtsi, Ukraine), OMT-800 (Mayaki, Ukraine) [30], AZT8 (Yevpatoria, Ukraine) [31], Takahashi BRC-250M (Uzhgorod, Ukraine), and National Astronomical Research Institute of Thailand (NARIT, Thailand) [32]. The observational conditions for the experiments were specially selected in such a way that the resulting series of CCD frames contained a variety of typical image forms of the studied SSOs [6].

The developed computational method was successfully used during the processing of test series of CCD frames. With this fact, the method of automated formation of a typical image form has confirmed its practical necessity within the framework of the main hypothesis put forward.

## 5. Results of investigating the automated formation of a typical form of a digital image of the objects under study on the frames

### 5.1. Selecting single images of objects and excluding images that are distorted by a coma from the list

The original blurred images of the studied objects on a series of CCD frames can take a completely different image form from frame to frame in the series (Fig. 1).

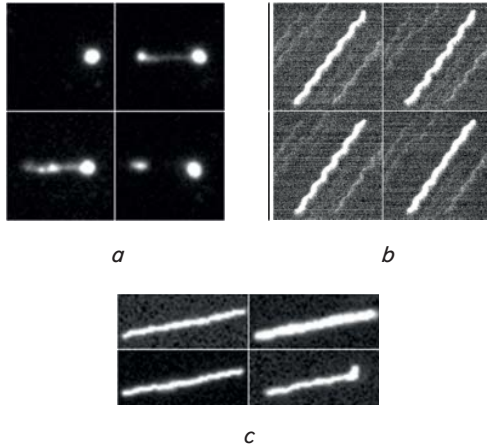


Fig. 1. Examples of blurred images of objects on a series of 4 CCD frames: *a* – when daily observation is disrupted; *b* – in case of inaccuracies in tracking an object; *c* – with gusts of wind

The typical image of the object under study on the CCD frame is evaluated according to  $N_{sel}$  selected single images. To do this, a list of bright images of the objects of the frame is compiled, that is, images with the aperture (total) brightness of the pixels of single images of objects  $A_{\Sigma m}^*$ , which meets the condition:

$$A_{\Sigma m}^* \geq (10 \div 20) \sigma_{noise}, \quad (1)$$

where  $\sigma_{noise}$  is an RMS estimate of the brightness of the background of the CCD frame;

$$A_{\Sigma m}^* = \sum_{l=1}^{Nsm} (A_{l(i,k)m}^* - C_{fm}) - \text{aperture (total) brightness of the pixels of the } m\text{-th single image of the object;}$$

$A_{l(i,k)m}^*$  is the brightness of the  $l(i, k)$ -th pixel of the set  $\Omega_{\Sigma m}$  of the  $m$ -th single image of the object;

$l(i, k)$  is the number of the pixel  $l$  in the set  $\Omega_{\Sigma m}$ , which is a function of the numbers of the  $ik$ -th pixel on the frame;

$C_{fm}$  is the average brightness of the background substrate of the CCD frame (local or on the frame as a whole).

For each image from the list of bright images of objects, the eccentricity  $\epsilon_m$  of the object's image is calculated:

$$\epsilon_m = \frac{m_{20} + m_{02} - \sqrt{m_{20} - m_{02} + 4m_{11}^2}}{m_{20} + m_{02} + \sqrt{m_{20} - m_{02} + 4m_{11}^2}}, \quad (2)$$

where

$$m_{20} = \sum_{l=1}^{Nsm} (A_{l(i,k)m}^* - C_{fm}) (x_{l(i,k)m} - X_0)^2, \quad (3)$$

$$m_{02} = \sum_{l=1}^{Nsm} (A_{l(i,k)m}^* - C_{fm}) (y_{l(i,k)m} - Y_0)^2, \quad (4)$$

$$m_{11} = \sum_{l=1}^{Nsm} (A_{l(i,k)m}^* - C_{fm}) (x_{l(i,k)m} - X_0) (y_{l(i,k)m} - Y_0) \quad (5)$$

– second-order moments;

$$X_0 = \frac{\sum_{l=1}^{Nsm} (A_{l(i,k)m}^* - C_{fm}) x_{l(i,k)m}}{A_{\Sigma m}^*}, \quad (6)$$

$$Y_0 = \frac{\sum_{l=1}^{Nsm} (A_{l(i,k)m}^* - C_{fm}) y_{l(i,k)m}}{A_{\Sigma m}^*} \quad (7)$$

– moments of the first order;

$x_{l(i,k)m}$ ,  $y_{l(i,k)m}$  are the coordinates of the  $l(i, k)$ -th pixel of the  $m$ -th single image of the object.

We also calculate the length  $L_m$  of the image of the object:

$$L_m = \sqrt{(x_{mmax} - x_{mmin})^2 + (y_{mmax} - y_{mmin})^2}, \quad (8)$$

where  $x_{mmax}$ ,  $y_{mmax}$ ,  $x_{mmin}$ ,  $y_{mmin}$  are the minimum and maximum values of the abscissa and ordinates of the  $m$ -th IFPA.

From the list of bright images of objects, we exclude images for which the estimate of eccentricity  $\epsilon_m$  and length  $L_m$  does not meet the conditions:

$$\epsilon_m > \gamma_\epsilon, \quad (9)$$

$$\frac{|L_m - L_{\gamma/2}|}{L_{\gamma/2}} < \gamma_L, \quad (10)$$

where  $\gamma_\epsilon = 0.6$  is the limit permissible value of the eccentricity;

$L_{\gamma/2}$  is the median value of the length of bright images of objects;

$\gamma_L = 0.1$  is the permissible relative deviation of the length of the image of objects.

As a criterion for the distortion of a single image of an object by a coma, the form parameter  $\sigma_{Gm}$  of the  $m$ -th image of the object is selected. The value of the median  $\sigma_{Gm\ell/2}$  estimates of the form parameter of the Gaussian sections of the single image of the object is taken as an assessment of the form parameter  $\sigma_{Gm}$  of the  $m$ -th image:

$$\sigma_{Gm} = \sigma_{Gm\ell/2}, \quad (11)$$

where  $\ell$  is the cross-section number of a single image of the object.

The list of bright images of objects is ordered in ascending order of the form parameter  $\sigma_{Gm}$ . Images of objects that meet the following condition are excluded from the list of single images of objects:

$$\sigma_{Gm} > \sigma_{G\%2}, \tag{12}$$

where  $\sigma_{G\%2}$  is the median value of the form parameter of single images of objects on the digital frame.

To estimate the form parameter  $\sigma_{Gm\ell}$  of the Gaussians of sections of a single image of an object, the image of the  $m$ -th object is divided along the semi-major axis into  $N_{segm}$  segments of  $\Delta x_{seg}$  pixels wide. Segmentation is carried out in the coordinate system (CS) associated with the image of the object. The CS center coincides with the center of the image of the object. The coordinates  $x_{cm}$ ,  $y_{cm}$  of the center of the image are defined by expressions given in [33]:

$$x_{cm} = \frac{\sum_{l(i,k)}^{NSm} x_{l(i,k)m} (A_{l(i,k)m}^* - C_{fm})}{\sum_{l(i,k)}^{NSm} (A_{l(i,k)m}^* - C_{fm})}, \tag{13}$$

$$y_{cm} = \frac{\sum_{l(i,k)}^{NSm} y_{l(i,k)m} (A_{l(i,k)m}^* - C_{fm})}{\sum_{l(i,k)}^{NSm} (A_{l(i,k)m}^* - C_{fm})}. \tag{14}$$

The object image's CS abscissa axis is rotated relative to the abscissa axis of the frame CS at angle  $\omega_m$ :

$$\omega_m = \frac{1}{2} \arctan \frac{2m_{11}}{m_{20} - m_{02}}, \tag{15}$$

where

$$m_{20} = \sum_{l(i,k)}^{NSm} y_{l(i,k)m} (A_{l(i,k)m}^* - C_{fm}) (x_{l(i,k)m} - x_{cm})^2, \tag{16}$$

$$m_{02} = \sum_{l(i,k)}^{NSm} y_{l(i,k)m} (A_{l(i,k)m}^* - C_{fm}) (y_{l(i,k)m} - y_{cm})^2, \tag{17}$$

$$m_{11} = \sum_{l(i,k)}^{NSm} y_{l(i,k)m} (A_{l(i,k)m}^* - C_{fm}) (x_{l(i,k)m} - x_{cm}) (x_{l(i,k)m} - x_{cm}) \tag{18}$$

– second-order moments [34].

The number of segments  $N_{segm}$  is defined by the expression:

$$N_{segm} = \frac{L_m}{\Delta x_{seg}}. \tag{19}$$

During the studies, the width of the segment  $\Delta x_{seg}$  was set to 2÷3 pixels. The pixels of a single image of the  $m$ -th object are considered to belong to the  $\ell$ -th segment  $\Omega_{segm\ell}$  if the following condition is met:

$$\ell \Delta x_{seg} \leq x_{l(i,k)m} < (\ell+1) \Delta x_{seg}. \tag{20}$$

The form parameter of the Gaussian of the  $\ell$ -section  $\sigma_{Gm\ell}$  of the image of the  $m$ -th object is calculated as an element of the vector of OLS evaluation [34] of parameters  $\Theta_{\sigma m\ell} = (\sigma_{Gm\ell}, A_{Gm\ell}, y_{0m\ell})$  using ALM [35] to minimize the functionality:

$$F_{\Delta Ag}(\Theta_{\sigma m\ell}) = \sum_{l(i,k)m=1}^{N_{segm\ell}} (A_{l(i,k)m}^* - C_{fm} - A_{S(l(i,k)m)}(\Theta_{\sigma m\ell}))^2 \rightarrow \min, \tag{21}$$

where  $A_{S(l(i,k)m)}(\Theta_{\sigma m\ell}) = A_{Gm\ell} \exp\left\{-\frac{1}{2\sigma_{Gm\ell}^2} (y_{l(i,k)m} - y_{0m\ell})^2\right\}$  is the

model brightness of the pixels of the  $\ell$ -th segment of the blurred image of the  $m$ -th object;

$N_{segm\ell}$  is the number of pixels in the  $\ell$ -th segment of a single image of the  $m$ -th object;

$A_{Gm\ell}$  – model amplitude of the Gaussian in the  $\ell$ -th segment;

$y_{0m\ell}$  is the coordinate of the reference center of the Gaussian in the  $\ell$ -th segment along the ordinate axis.

The generated list of bright images of objects is ordered in descending order of aperture (total) brightness. An ordered set excludes 10÷20 % of the images of objects with the highest aperture brightness. From the resulting set,  $N_{sel}$  of the brightest images of the objects shall be selected. In other words, the first single image of the object in the ordered set selected for evaluation of the typical form on the digital frame has a number equal to  $(0.1\div 0.2)N_S$ . The number of the last selected single image of the object is  $(0.1\div 0.2)N_S + N_{sel}$ .

### 5. 2. Constructing a rectangular area of the selected single images of objects and then evaluating their offset

From the selected single images of objects  $\Omega_{Sm}$ , a rectangular region of  $N_{Sx} \times N_{Sy}$  pixels is constructed. The brightness values  $A_{ikm}$  of the  $ik$ -th pixel of the rectangular region of the  $m$ -th single image of the object are specified:

$$A_{ikm} = \begin{cases} A_{l(i,k)m}^* - C_{fm}, & \forall l \in \Omega_{Sm}, \\ 0, & \forall l \notin \Omega_{Sm}. \end{cases} \tag{22}$$

The size of the rectangular area  $N_{Sx} \times N_{Sy}$  is determined by twice the sum of the maximum size of  $N_{Smaxx}$ ,  $N_{Smaxy}$  of the frame IFPA and the size of the border  $N_{borx}$ ,  $N_{bory}$  along the abscissa and ordinate axes, respectively:

$$N_{Sx} = 2(N_{Smaxx} + N_{borx}), \tag{23}$$

$$N_{Sy} = 2(N_{Smaxy} + N_{bory}). \tag{24}$$

During the studies and subsequent analysis, the values of the size of the border  $N_{borx}$  and  $N_{bory}$  were obtained empirically and are equal to five pixels. To calculate the average image of an object from selected single images, the offsets between these images are pre-calculated. Determining the mutual offset  $N_{sel}-1$  of the selected single images of objects is performed relative to a single image of the object with the maximum intra-frame correlation. The offset between the selected single images is calculated from the coordinates of the maximum linear coefficient correlation  $\rho_{1m}$  [33]. The value of the linear correlation coefficient of two images depends on their mutual displacement. The maximum of the coefficient is reached when the images are fully combined, and the maximum value characterizes the degree of linear similarity of the studied images. The linear correlation coefficient is calculated in steps of one pixel. Preliminary studies have shown that this step was sufficient to assess the typical profile of the object's image on the digital frame.

The value of the  $ik$ -th pixel of the linear correlation coefficient  $\rho_{ik1m}$  for the image of the object with the maximum intra-frame correlation and the  $m$ -th selected single image of the object is determined by the expression given in [33]:

$$\rho_{ik1m} = \frac{\sum_{i=1}^{N_{sx}} \sum_{k=1}^{N_{sy}} (A_{ik1} - \bar{A}_1)(A_{(i-k)m} - \bar{A}_m)}{\sqrt{\sum_{i=1}^{N_{sx}} \sum_{k=1}^{N_{sy}} (A_{ik1} - \bar{A}_1)^2 \sum_{i=1}^{N_{sx}} \sum_{k=1}^{N_{sy}} (A_{ikm} - \bar{A}_m)^2}}, \quad (25)$$

where  $A_{ik1}$ ,  $A_{ikm}$  is the brightness value of the  $ik$ -th pixel of the rectangular area of the image of the object with the maximum intra-frame correlation and the  $m$ -th selected single image of the object, respectively;

$$\bar{A}_m = \frac{1}{N_{sx} N_{sy}} \sum_{i=1}^{N_{sx}} \sum_{k=1}^{N_{sy}} A_{ikm} \quad (26)$$

is the average brightness of the rectangular area of the  $m$ -th selected single image of the object.

From the  $x_{MAXm}$ ,  $y_{MAXm}$  coordinates of the maximum value of the linear correlation coefficient  $\rho_{1m}$ , the offset for the  $m$ -th selected single image of the object is calculated:

$$x_{shiftm} = x_{MAXm} - \frac{1}{2} N_{sx} + (x_{mmin} - x_{1min}), \quad (27)$$

$$y_{shiftm} = y_{MAXm} - \frac{1}{2} N_{sy} + (y_{mmin} - y_{1min}), \quad (28)$$

where  $x_{mmin}$ ,  $y_{mmin}$  are the minimum values of the abscissa and ordinate of the  $m$ -th IFPA.

For each, for example,  $n$ -th, of  $N_{first}$  selected single images of objects,  $N_{sel}-1$  of the maximum values  $\rho_{MAXnm}$  of linear correlation coefficients is determined. The sum  $\rho_{\Sigma n}$  of the maximum values of the linear correlation coefficients for the first selected single images of objects is calculated:

$$\rho_{\Sigma n} = \sum_{m=1}^{N_{sel}-1} \rho_{MAXnm}. \quad (29)$$

A single image of an object with the maximum intra-frame correlation is the  $n$ th first selected single image of the object, for which the sum  $\rho_{\Sigma n}$  of the maximum values of the linear correlation coefficients has the greatest value:

$$j_{MAX} = \arg \max_n \rho_{\Sigma n}. \quad (30)$$

When one defines a typical image form for a digital frame object, the selected single images of objects are normalized. Normalization is necessary to eliminate differences in the aperture (PSF) brightness of object images when calculating the average or median of selected single images. The brightness of the pixels of the normalized single image of the  $m$ -th IFPA object is calculated according to the expression:

$$A_{l(i,k)m}^n = \frac{A_{l(i,k)m}^* - C_{fm}}{A_{\Sigma m}^*}, \quad (31)$$

where  $A_{l(i,k)m}^n$  is the normalized brightness of the  $l(i,k)$ -th pixel of the  $m$ -th IFPA.

### 5.3. Computational method of automated formation of the typical form of the image of an object on a series of digital frames

The set of pixels of a typical digital frame image  $\Omega_{img}$  includes pixels for which the brightness values  $A_{l(i,k)m}^n$  of at least two of  $N_{sel}$  normalized single images of objects are determined. The brightness value of the  $l(i,k)$ -th pixel of the typical image of the digital frame is calculated as the average brightness value of the normalized single images:

$$A_{l(i,k)img} = \frac{1}{N_{l(i,k)}} \sum_{m=1}^{N_{l(i,k)}} A_{l(i,k)m}^n, \quad (32)$$

where  $N_{l(i,k)}$  is the number of normalized single images of objects for which brightness values are defined in the  $l(i,k)$ -th pixel.

The resulting values of the brightness of the pixels of the typical image of the digital frame are standardized by the sum of the brightness of the pixels of the typical image of the digital frame:

$$A_{l(i,k)img}^n = \frac{A_{l(i,k)img}}{\sum_{l=1}^{N_{img}} A_{l(i,k)img}}, \quad (33)$$

where  $N_{img}$  is the number of pixels of the set  $\Omega_{img}$ .

The calculation of  $x_{cimg}$ ,  $y_{cimg}$  coordinates of the binding center of the typical image of the digital frame is determined by the expression:

$$x_{cimg} = \frac{\sum_{l=1}^{N_{img}} x_{l(i,k)img} A_{l(i,k)img}^n}{\sum_{l=1}^{N_{img}} A_{l(i,k)img}^n}, \quad (34)$$

$$y_{cimg} = \frac{\sum_{l=1}^{N_{img}} y_{l(i,k)img} A_{l(i,k)img}^n}{\sum_{l=1}^{N_{img}} A_{l(i,k)img}^n}. \quad (35)$$

The developed computational method of automated formation of the typical form of an image of the object on a series of digital frames is the following sequence of operations:

1. Select  $N_{sel}$  single images of objects to compute a typical image on a digital frame according to conditions (1), (9)÷(11).
2. Form rectangular areas for  $N_{sel}$  selected single images of objects (22).
3. Calculate the linear correlation coefficients  $\rho_{1m}$  for  $N_{sel}$  rectangular regions of single images of objects according to expression (25).
4. Determine the offsets of  $N_{sel} - 1$  selected single images of objects relative to a single image of an object with maximum intra-frame correlation according to expressions (27) and (28).
5. Standardize  $N_{sel}$  selected single images of objects according to expression (31).
6. Determine the brightness of the pixels of a typical image of a digital frame according to expressions (32) and (33).
7. Refine the typical form of the image of the digital frame.
  - 7.1. For  $N_{sel}$  normalized selected single images of objects, linear correlation coefficients with the typical image of the digital frame (25) are calculated.

7. 2. The selected normalized single images of objects are sorted in descending order of the maximum values of the linear correlation coefficients  $\rho_m$ .

7. 3. From the sorted list of selected single images of objects, the first  $N_{val}$  valid images are selected.

7. 4. For  $N_{val}$  valid images of objects, steps 2–6 are repeated.

8. For the resulting typical image of the digital frame, the values  $x_{cimg}$ ,  $y_{cimg}$  of the coordinates of the binding center are calculated according to expressions (34) and (35).

Our studies of the effectiveness of using a typical image of the object were carried out on the frames of the telescopes KOS “Sazhen-S” (Dunaevtsy), OMT-800 (Mayaki), AZT8 (Evpatoria), and Takahashi BRC-250M (Uzhgorod). Below, Fig. 2–5, *a* show the typical examples of images blurred by the natural movement of objects found on the frames from these observatories. As well as images of the standard image of the frame formed by the developed method (Fig. 2–5, *b*) and the analytical model of the blurred image of an object [2] (Fig. 2–5, *c*).

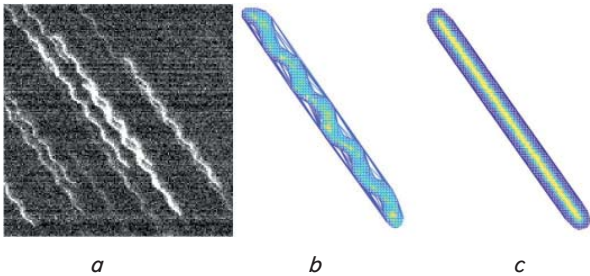


Fig. 2. Fragment of the frame of the KOS telescope “Sazhen-S”: *a* – the original image; *b* – the generated typical image; *c* – analytical image model

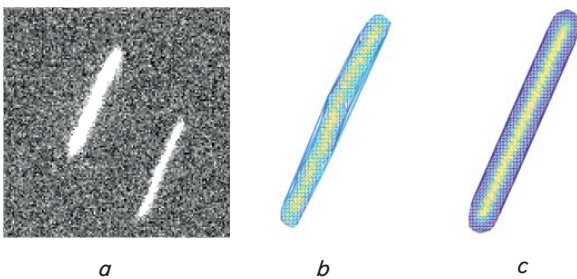


Fig. 3. Fragment of the frame of the OMT-800 telescope: *a* – the original image; *b* – the generated typical image; *c* – analytical image model

As a criterion for efficiency, the RMS  $\sigma_{\Delta A_j}$  of the difference between the experimental and model brightness of the pixels of the image of the *j*-th blurred object on the frame was calculated:

$$\sigma_{\Delta A_j} = \sqrt{\frac{1}{N_j} \sum_{i=1}^{N_j} (A_i^* - A_i)^2}, \quad (36)$$

where  $A_i^*$  and  $A_i$  is the experimental and model brightness of the *i*-th pixel of the image of the extended object;

$N_j$  is the number of pixels in the image of the *j*-th extended object on the frame.

RMS difference in brightness  $\sigma_{\Delta A_j}$  of the image of the *j*-th blurred object was calculated for two model values of

the brightness of the pixels of the image. In the first case, the model brightness was calculated from the formed typical image of the object on the frame, in the second – from the analytical model of the blurred image of the object [2].

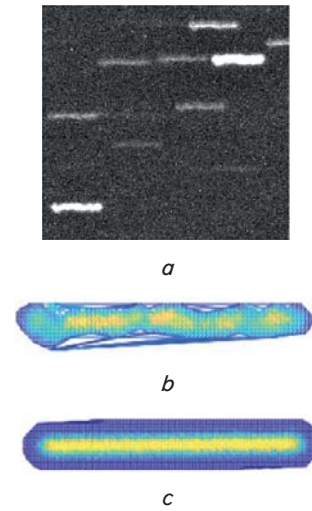


Fig. 4. Fragment of the frame of the AZT8 telescope: *a* – the original image; *b* – the generated typical image; *c* – analytical image model

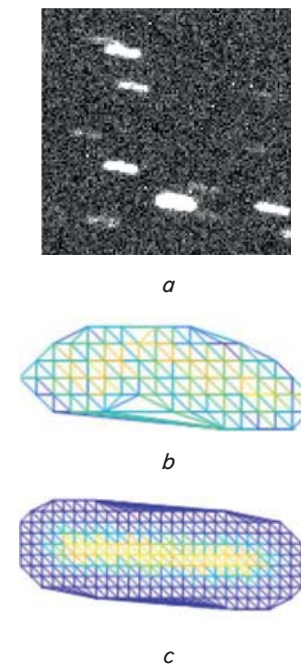


Fig. 5. Fragment of the frame of the telescope Takahashi BRC-250M: *a* – the original image; *b* – the generated typical image; *c* – analytical image model

Table 1 gives the RMS characteristics  $\sigma_{\Delta A_j}$  of the difference in the experimental and model brightness of the pixels of all images of blurred objects in the frame. Namely, the average RMS value  $\sigma_{\Delta A}$  of the difference in brightness  $M\sigma_{\Delta A}$  in the frame (column 3); the value of the median  $M_{1/2}\sigma_{\Delta A}$  in the frame (column 4); the maximum  $\max\sigma_{\Delta A}$  and the minimum  $\min\sigma_{\Delta A}$  RMS values of the brightness difference in the frame (columns 5–6).

Table 1

RMS characteristics of model and experimental brightness on the frame

| Telescope          | Number of blurred objects | Model brightness | $M\sigma_{\Delta A}$ , ADU | $M_{1/2}\sigma_{\Delta A}$ , ADU | $\max\sigma_{\Delta A}$ , ADU | $\min\sigma_{\Delta A}$ , ADU |
|--------------------|---------------------------|------------------|----------------------------|----------------------------------|-------------------------------|-------------------------------|
| KOS «Sazhen-S»     | 149                       | Typical image    | 62.77                      | 12.86                            | 559.48                        | 2.28                          |
|                    |                           | Analytical model | 175.28                     | 36.13                            | 1,053.61                      | 2.22                          |
| OMT-800            | 62                        | Typical image    | 4.41                       | 2.4                              | 19.29                         | 0.3562                        |
|                    |                           | Analytical model | 7.89                       | 4.41                             | 30.36                         | 0.6983                        |
| AZT8               | 123                       | Typical image    | 23.49                      | 3.21                             | 1,357.32                      | 0.23                          |
|                    |                           | Analytical model | 66.28                      | 5.64                             | 1,595.64                      | 0.42                          |
| Takahashi BRC-250M | 417                       | Typical image    | 12.06                      | 3.26                             | 242.92                        | 0.33                          |
|                    |                           | Analytical model | 13.63                      | 3.77                             | 1,057.19                      | 1.21                          |

Based on the data in Table 1, one can conclude that the effectiveness of the developed method for forming a typical image shape of an object is much higher (up to 54 %) in relation to using an analytical image model [2].

**6. Discussion of results of investigating the automated formation of the standard form of the image of objects on a series of digital frames**

Within the framework of this work, the possibility of automated formation of a typical form of the image of an object on a series of digital frames was investigated. As a result of our studies, examples of blurred images were analyzed (Fig. 1), as well as typical conditions for their appearance. Existing methods of image processing and machine vision [8] were also analyzed. Basically, they are aimed at detecting objects [3], their movement, and estimating image and trajectory parameters [6]. However, the accuracy and quality of processing by such methods directly depended on the accuracy and quality of the original image of the object under study on the CCD frame.

Therefore, within the framework of the CoLiTec research project [29], the developed method of automated formation of a typical form of a digital image was tested.

As the study showed, the application of the developed method significantly affects the quality and accuracy (up to 54 % improvement) of a number of tasks. Namely, data acquisition [36], image processing and machine vision [3] (detection of images of objects and assessment of their parameters [37], detection of the movement of objects and assessment of the parameters of motion trajectories [18]). This indicator clearly indicates that the tasks have been successfully solved.

Analysis of the results of our studies showed an increase in the probability of identification of the studied objects with those already known from the list of cataloged ones [5]. In addition, the CPCD and accuracy of the assessment of image parameters increased by 15–20 % after preliminary processing before the main processing method (Table 1).

These results are due primarily to the formation of rectangular areas for selected single images of objects (22) followed by their normalization (31). In addition, an important factor is determining the linear correlation coefficients for rectangular areas of single images of objects (25). This has made it possible to calculate the coordinate values of the reference center (34)–(35) for the subsequent construction of a typical image.

Thus, the developed computational method makes it possible to successfully form a typical form of a digital image

of each object on the frame under an automated mode. The formed standard form is based on the data of all digital images of the same object on each frame of the series. And the use of the developed method makes it possible to distinguish the objects under study against the background of the noise of the substrate and improve the segmentation of images, thereby reducing the number of false detections.

The limitation of this study is the computing power of the equipment involved in processing. The possibility of using the developed method is limited by the fact that it cannot be executed immediately upon acquiring the first CCD frame of the series. This means that a series of CCD frames must be formed before applying the developed method. Also important is the issue of security [38], namely the encryption of input digital data. In this case, the developed method cannot be used without an additional decoding algorithm.

The disadvantage of the study is the fact that in the case when all the frames are “perfect” and do not have blurs during shooting, the use of this method is impractical due to additional computational costs. However, the solution to this problem is to add a signal-to-noise ratio (SNR) condition to the processing algorithm to exclude computational method operations from it.

Further research should focus on the application of the developed computational method of automated formation of a typical form of a digital image as a preliminary stage of processing. It will also be necessary to analyze (including Wavelet analysis [39] and the forecasting method [40]) its impact on the basic methods of image processing, for example, coordinated filtering [2, 41], assessment of the parameters of the image of the object (positional coordinates [3, 37], glitter [5]).

**7. Conclusions**

1. A selection of single images of objects was performed. For each image, the eccentricity  $\epsilon_m$  and the length of  $L_m$  were calculated. A criterion was also selected for the distortion of a single image of the object by the coma. Based on the eccentricity  $\epsilon_m$ , the length  $L_m$  and the distortion criteria, we excluded from the list the images distorted by coma, in accordance with the conditions of exceeding the permissible limit value of eccentricity and the relative deviation of the length of the image of objects.

2. The construction of rectangular areas of the selected single images of objects allowed us to make the most accurate assessment of their displacement. During the studies and subsequent analysis, the values of the size of the border  $N_{borx}$  and  $N_{bory}$  were obtained empirically and are equal to

five pixels. The calculations have made it possible to perform the normalization, which is necessary to eliminate differences in the aperture (PSF) brightness of images of objects when calculating the average or median of the selected single images.

3. Owing to preliminary calculations, a computational method was developed for the automated formation of a typical form of the image of an object on a series of digital frames. The final step of this method is to determine the coordinates  $x_{cimg}$ ,  $y_{cimg}$  of the reference center. Thus, the construction of a typical form of the image of objects makes it possible in 96 % of cases to select the true object on each frame of the series. This significantly affects the quality and accuracy (an improvement of 15–20 %) of the subsequent identification with cataloged objects and the execution of a number of image processing tasks.

---

#### Conflicts of interest

---

The authors declare that they have no conflicts of interest in relation to the current study, including financial, personal, authorship, or any other, that could affect the study and the results reported in this paper.

---

#### Funding

---

The study was conducted without financial support.

---

#### Data availability

---

Manuscript has no associated data.

---

#### References

- Smith, G. E. (2010). Nobel Lecture: The invention and early history of the CCD. *Reviews of Modern Physics*, 82 (3), 2307–2312. doi: <https://doi.org/10.1103/revmodphys.82.2307>
- Khlamov, S., Vlasenko, V., Savanevych, V., Briukhovetskiy, O., Trunova, T., Chelombitko, V., Tabakova, I. (2022). Development of computational method for matched filtration with analytical profile of the blurred digital image. *Eastern-European Journal of Enterprise Technologies*, 5 (4 (119)), 24–32. doi: <https://doi.org/10.15587/1729-4061.2022.265309>
- Steger, C., Ulrich, M., Wiedemann, C. (2018). *Machine vision algorithms and applications*. John Wiley & Sons, 516.
- Cavuoti, S., Brescia, M., Longo, G. (2012). Data mining and knowledge discovery resources for astronomy in the web 2.0 age. *Software and Cyberinfrastructure for Astronomy II*. doi: <https://doi.org/10.1117/12.925321>
- Zhang, Y., Zhao, Y., Cui, C. (2002). Data mining and knowledge discovery in database of astronomy. *Progress in Astronomy*, 20 (4), 312–323.
- Mykhailova, L., Savanevych, V., Sokovikova, N., Bezkrivnyy, M., Khlamov, S., Pogorelov, A. (2014). Method of maximum likelihood estimation of compact group objects location on CCD-frame. *Eastern-European Journal of Enterprise Technologies*, 5 (4 (71)), 16–21. doi: <https://doi.org/10.15587/1729-4061.2014.28028>
- Kuz'min, S. Z. (2000). *Tsifrovaya radiolokatsiya. Vvedenie v teoriyu*. Kyiv: Izdatel'stvo KviTS, 428.
- Khlamov, S., Savanevych, V. (2020). Big Astronomical Datasets and Discovery of New Celestial Bodies in the Solar System in Automated Mode by the CoLiTec Software. *Knowledge Discovery in Big Data from Astronomy and Earth Observation*, 331–345. doi: <https://doi.org/10.1016/b978-0-12-819154-5.00030-8>
- Akhmetov, V., Khlamov, S., Dmytrenko, A. (2018). Fast Coordinate Cross-Match Tool for Large Astronomical Catalogue. *Advances in Intelligent Systems and Computing III*, 3–16. doi: [https://doi.org/10.1007/978-3-030-01069-0\\_1](https://doi.org/10.1007/978-3-030-01069-0_1)
- Vavilova, I. B., Shatokhina, S. V., Pakuliak, L. K., Yizhakevych, O. M., Eglitis, I., Andruk, V. M., Protsyuk, Yu. I. (2019). Astrometry and photometry of asteroids from the UkrVO database of astroplates. *Proceedings of the International Astronomical Union*, 15 (S364), 239–245. doi: <https://doi.org/10.1017/s1743921322000047>
- Dearborn, D. P. S., Miller, P. L. (2014). Defending Against Asteroids and Comets. *Handbook of Cosmic Hazards and Planetary Defense*, 1–18. doi: [https://doi.org/10.1007/978-3-319-02847-7\\_59-1](https://doi.org/10.1007/978-3-319-02847-7_59-1)
- Klette, R. (2014). *Concise computer vision. An Introduction into Theory and Algorithms*. Springer, 429. doi: <https://doi.org/10.1007/978-1-4471-6320-6>
- Savanevych, V. E., Khlamov, S. V., Akhmetov, V. S., Briukhovetskiy, A. B., Vlasenko, V. P., Dikov, E. N. et al. (2022). CoLiTecVS software for the automated reduction of photometric observations in CCD-frames. *Astronomy and Computing*, 40, 100605. doi: <https://doi.org/10.1016/j.ascom.2022.100605>
- Khlamov, S., Savanevych, V., Briukhovetskiy, O., Oryshych, S. (2016). Development of computational method for detection of the object's near-zero apparent motion on the series of ccd-frames. *Eastern-European Journal of Enterprise Technologies*, 2 (9 (80)), 41–48. doi: <https://doi.org/10.15587/1729-4061.2016.65999>
- Vavilova, I., Pakuliak, L., Babyk, I., Elyiv, A., Dobrycheva, D., Melnyk, O. (2020). Surveys, Catalogues, Databases, and Archives of Astronomical Data. *Knowledge Discovery in Big Data from Astronomy and Earth Observation*, 57–102. doi: <https://doi.org/10.1016/b978-0-12-819154-5.00015-1>
- Minaee, S., Boykov, Y. Y., Porikli, F., Plaza, A. J., Kehtarnavaz, N., Terzopoulos, D. (2021). Image Segmentation Using Deep Learning: A Survey. *IEEE Transactions on Pattern Analysis and Machine Intelligence*, 44 (7). doi: <https://doi.org/10.1109/tpami.2021.3059968>
- Kobzar', A. I. (2006). *Prikladnaya matematicheskaya statistika. Dlya inzhenerov i nauchnykh rabotnikov*. Moscow: FIZMATLI, 816.

18. Khlamov, S., Savanevych, V., Tabakova, I., Trunova, T. (2022). The astronomical object recognition and its near-zero motion detection in series of images by in situ modeling. 2022 29th International Conference on Systems, Signals and Image Processing (IWSSIP). doi: <https://doi.org/10.1109/iwssip55020.2022.9854475>
19. Akhmetov, V., Khlamov, S., Tabakova, I., Hernandez, W., Nieto Hipolito, J. I., Fedorov, P. (2019). New approach for pixelization of big astronomical data for machine vision purpose. 2019 IEEE 28th International Symposium on Industrial Electronics (ISIE). doi: <https://doi.org/10.1109/isie.2019.8781270>
20. Khlamov, S., Tabakova, I., Trunova, T. (2022). Recognition of the astronomical images using the Sobel filter. 2022 29th International Conference on Systems, Signals and Image Processing (IWSSIP). doi: <https://doi.org/10.1109/iwssip55020.2022.9854425>
21. Bishop, C. M. (2013). Model-based machine learning. *Philosophical Transactions of the Royal Society A: Mathematical, Physical and Engineering Sciences*, 371 (1984), 20120222. doi: <https://doi.org/10.1098/rsta.2012.0222>
22. Burger, W., Burge, M. (2010). Principles of digital image processing: core algorithms. Springer, 332. doi: <https://doi.org/10.1007/978-1-84800-195-4>
23. Gonzalez, R., Woods, R. (2018). Digital image processing. New York, NY: Pearson, 1168.
24. Rubin, B. (2015). Introduction to Radon transforms. With Elements of Fractional Calculus and Harmonic Analysis. *Encyclopedia of Mathematics and its Applications*. Cambridge University Press, 596.
25. Brandt, A. (2011). Noise and vibration analysis: signal analysis and experimental procedures. John Wiley & Sons, 464. doi: <https://doi.org/10.1002/9780470978160>
26. Dadkhah, M., Lyashenko, V. V., Deineko, Z. V., Shamshirband, S., Jazi, M. D. (2019). Methodology of wavelet analysis in research of dynamics of phishing attacks. *International Journal of Advanced Intelligence Paradigms*, 12 (3/4), 220. doi: <https://doi.org/10.1504/ijaip.2019.098561>
27. Jorgensen, B. (2012). Statistical properties of the generalized inverse Gaussian distribution. Springer, 188. doi: <https://doi.org/10.1007/978-1-4612-5698-4>
28. Lemur software. CoLiTec. Available at: <https://colitec.space/>
29. Khlamov, S., Savanevych, V., Briukhovetskiy, O., Pohorelov, A., Vlasenko, V., Dikov, E. (2018). CoLiTec Software for the Astronomical Data Sets Processing. 2018 IEEE Second International Conference on Data Stream Mining & Processing (DSMP). doi: <https://doi.org/10.1109/dsmp.2018.8478504>
30. Kashuba, S., Tsvetkov, M., Bazyey, N., Isaeva, E., Golovnia, V. (2018). The Simeiz plate collection of the ODESSA astronomical observatory. *Proceedings of the XI Bulgarian-Serbian Astronomical Conference*, 207–216.
31. Molotov, I. et al. (2009). ISON worldwide scientific optical network. *Fifth European Conference on Space Debris*, ESA.
32. Mingmuang, Y., Tummuangpak, P., Asanok, K., Jaroenjittichai, P. (2019). The mass distribution and the rotation curve of the Milky Way Galaxy using NARIT 4.5 m small radio telescope and the 2.3 m Onsala radio telescope. *Journal of Physics: Conference Series*, 1380 (1), 012028. doi: <https://doi.org/10.1088/1742-6596/1380/1/012028>
33. Soyfer, V. A. (Ed.) (2003). *Metody komp'yuternoy obrabotki izobrazheniy*. Moscow: Fizmatlit, 784.
34. Sergienko, A. B. (2011). *Tsifrovaya obrabotka signalov*. Sankt-Peterburg: BKhV-Peterburg, 768.
35. Le, D.-H., Pham, C.-K., Nguyen, T. T. T., Bui, T. T. (2012). Parameter extraction and optimization using Levenberg-Marquardt algorithm. 2012 Fourth International Conference on Communications and Electronics (ICCE). doi: <https://doi.org/10.1109/cce.2012.6315945>
36. Khlamov, S., Savanevych, V., Briukhovetskiy, O., Tabakova, I., Trunova, T. (2022). Data Mining of the Astronomical Images by the CoLiTec Software. *CEUR Workshop Proceedings*, 3171, 1043–1055.
37. Akhmetov, V., Khlamov, S., Khramtsov, V., Dmytrenko, A. (2019). Astrometric Reduction of the Wide-Field Images. *Advances in Intelligent Systems and Computing*, 896–909. doi: [https://doi.org/10.1007/978-3-030-33695-0\\_58](https://doi.org/10.1007/978-3-030-33695-0_58)
38. Buslov, P., Shvedun, V., Streltsov, V. (2018). Modern Tendencies of Data Protection in the Corporate Systems of Information Consolidation. 2018 International Scientific-Practical Conference Problems of Infocommunications. *Science and Technology (PIC S&T)*. doi: <https://doi.org/10.1109/infocommst.2018.8632089>
39. Baranova, V., Zeleniy, O., Deineko, Z., Bielcheva, G., Lyashenko, V. (2019). Wavelet Coherence as a Tool for Studying of Economic Dynamics in Infocommunication Systems. 2019 IEEE International Scientific-Practical Conference Problems of Infocommunications, *Science and Technology (PIC S&T)*. doi: <https://doi.org/10.1109/picst47496.2019.9061301>
40. Dombrovska, S., Shvedun, V., Streltsov, V., Husarov, K. (2018). The prospects of integration of the advertising market of Ukraine into the global advertising business. *Problems and Perspectives in Management*, 16 (2), 321–330. doi: [https://doi.org/10.21511/ppm.16\(2\).2018.29](https://doi.org/10.21511/ppm.16(2).2018.29)
41. Wang, J., Cai, D., Wen, Y. (2011). Comparison of matched filter and dechirp processing used in Linear Frequency Modulation. 2011 IEEE 2nd International Conference on Computing, Control and Industrial Engineering. doi: <https://doi.org/10.1109/cciug.2011.6008069>